Influence of the laser source pulsing frequency on the direct laser deposited Inconel 718 thin walls

Imbrogno, Stano; Alhuzaim, Abdullah; Attallah, Moataz M.

DOI:
10.1016/j.jallcom.2020.158095

Document Version
Peer reviewed version

Citation for published version (Harvard):
Imbrogno, S, Alhuzaim, A & Attallah, MM 2021, 'Influence of the laser source pulsing frequency on the direct laser deposited Inconel 718 thin walls', *Journal of Alloys and Compounds*, vol. 856, 158095. https://doi.org/10.1016/j.jallcom.2020.158095

Influence of the Laser Source Pulsing Frequency on the Direct Laser Deposited Inconel 718 Thin Walls

Stano Imbrogno[a], Abdullah Alhuzaim[a,b], Moataz M. Attallah*[a]

[a]School of Metallurgy and Material Sciences, University of Birmingham, Edgbaston, Birmingham B15 2TT, United Kingdom

[b]Mechanical Engineering Department, Jubail University College, Jubail Industrial City, Kingdom of Saudi Arabia.

*Corresponding author contact: m.m.attallah@bham.ac.uk , University of Birmingham.

Abstract: The Direct Laser Deposition (DLD) process has shown significant results in manufacturing due to its relevant flexibility to refurbish high-performance components (e.g. turbine blades or disks) or fabricating complex shaped parts. The solidification microstructure during the DLD process, is known to be controllable using different process parameters that induce changes in the grain structure, micro-segregation, and phase transformations. This work focuses on the effect the frequency of the pulsed laser has on the metallurgical characteristics of deposited thin walls. More specifically, the effect of three different pulsing rates (10Hz, 100Hz, 1000 Hz) during the deposition of the Nickel-based superalloys Inconel 718 has been studied and the results compared with parts produced by continuous wave laser mode. This work highlights how the pulsing rate significantly affected the thermal history, melt pool shape, grain size and its morphology, segregation region (Nb-enriched), and hardness. Finally, the microhardness was also evaluated and a correlation between the metallurgical characteristics and the pulsing rate was established.

Keywords: Direct Laser Deposition; pulsing laser; Inconel 718; microstructure

1. Introduction

Additive Manufacturing (AM) processes are creating interesting opportunities in producing high-performance structures, together with specifically designed metallurgical features. Among all the AM process, the Direct Laser Deposition (DLD) technique has been widely used for repairing or cladding mechanical components (e.g. turbine blade and blisks, hard coating for complex tools for mining). Moreover, the DLD also enables the fabrication of 3D near-net-shape parts directly from CAD models [1–3].

Generally, the process consists of a laser source that creates a melt pool on a substrate, while the metallic powder is delivered from a nozzle into the melt pool and fully melted. The laser head can be mounted on a cartesian system able to move on x, y and z directions, coupled with rotational support, in order to have 5-axis of degree of freedom, alternatively it is simply positioned at the end of an arm robot. In this contest, the Nickel base superalloy Inconel 718 is widely used in aerospace applications to produce high-performance components because of its good formability, high corrosion resistance, and excellent mechanical properties up to 650°C [4,5]. The Inconel 718 typically consists of a matrix, the γ phase (face-centered cubic FCC) structure that provides appropriate ductility and toughness at high temperatures. Furthermore, the strengthening of the alloy is guaranteed by the presence of the precipitation phase gamma prime γ' (Ni_3Al with spherical morphology) and gamma double prime γ'' (Ni_3Nb with disc morphology). This later has a metastable body-centred tetragonal structure that can be transformed into a coarse platelet stable orthorhombic δ phase, if exposed for a certain time at temperatures above 650 °C [6]. During the DLD process, the material undergoes rapid cooling and solidification, resulting in a refined dendritic microstructure. Concerning the Inconel 718, the fast Nb diffusion at the interface between the liquid and the solid phase

during solidification leads to the formation of significant interdendritic Nb segregation regions. These spots in the material are characterized by brittle intermetallic, and usually undesirable Laves phase (eutectic Laves phase/γ in the last stage of the solidification) [7]. The presence of the microsegregation is unavoidable during the welding process of the Inconel 718, as reported by Radhakrishna and Prasad Rao 1997 [8]. Indeed, the formation of the Laves phase is easier due to the microsegregation of elements present in the alloy, such as Nb, Ti, and Mo because of the non-equilibrium solidification conditions. The Laves phase is characterized by a hexagonal close-packed crystallographic structure and is usually represented by a concentration of Nb ranging from 10%-30%. It is generally known that the presence of this phase is not particularly desired due to the deleterious effect on the mechanical properties [9]. Different studies have shown that the formation and the presence of the Laves phase in the alloy deplete the matrix of the principal alloying elements (e.g. the Nb), which strongly contributes to the formation of the strengthening phases (e.g. γ' and γ'') of the material [4,9,10]. Moreover, the Laves phase, and in particular the interface region between this later and the matrix ,represents a nucleation point of cracks leading to the failure of the material when subjected to high or low cycle fatigue [11]. Due to the important role of the DLD process in the industrial environment, several studies were conducted to define a process strategy able to reduce and control the microsegregation formation. Antonsson and Fredriksson in 2003 studied the effect of the cooling rate on the solidification of Inconel 718, focusing their attention on the solidification sequence and the microstructural changes, as well as the Nb segregation. They discovered that the cooling rate has a significant effect on the type of microstructure that develops from the liquid phase, as well as on the segregation of the Nb. In detail, the coarseness of the matrix structure (γ phase) decreased when the cooling rate was increased, and the morphology changed from dendrites to cells.

They also measured the Nb segregation depending on the cooling rate, and showed that the percentage of Nb was lower at this higher cooling rate due to the improved solubility of this phase into the γ matrix [12]. Zhang et al. 2013 investigated the effect of ultrarapid cooling on the microstructure when the Inconel 718 alloy was used in the cladding process. They observed that the high cooling rate led to a reduction of the Laves phase and a variation in its morphology which was clearly refined and widely dispersed. In detail, the ultrarapid cooling induced a significant reduction of the constitutional supercooling, limiting the Nb segregation into the Laves phase [13]. Other researchers, such as Qi et al. 2009 and Zhang et al. 2013 analysed the effect of the different heat treatment on the microstructure, mechanical properties, and Nb segregation of the Inconel 718 produced by laser cladding. Qi et al. 2009 observed that the direct age could improve the strength of the material, due to the formation of the strengthening phases, but the ductility was strongly compromised due to the presence of the Laves phase. The homogenized solution treatment and ageing were able to completely dissolve the Laves phase into the matrix, but these treatments compromised the microstructure due to the significant grain growth [14]. Zhang et al 2013 obtained similar results which also showed the amount of the Laves phase was different from the region close to the substrate, and the top region of the deposited material [13]. As highlighted by Ma et al. 2015, and Zhai et al. 2019, the process parameters such as scan speed and the power can affect the microstructure and the microsegregation [15,16]. Zhai et al. 2019 showed that a combination of power and scan speed could change the cooling rate, leading to fast cooling and an exceptionally fine microstructure with lower Nb segregation. Ma et al. 2015 defined a map that showed the morphology changes from cells to dendritic microstructure, depending on the power and scan speed, as well as the hardness variation depending on the energy density. Kong et al. 2019 studied the effect of different Nb-content in the IN718 alloy on the

metallurgical characteristics and the mechanical properties. They noticed that if the Nb content within the alloy is lower than 3-4%, there is no formation of Laves phase and significant segregation regions. Moreover, the increase in the Nb content enhanced the formation of finer microstructure as well as the presence of the Laves phase improving thus the strength of the material [17]. New studies revealed the effectiveness of the pulsed laser during the laser metal deposition in terms of Nb segregation modification, as well as the surface roughness in the produced parts. Gharbi et al. 2014 analysed the use of pulsed regime laser, versus the continuous regime on the surface showing that the use of a pulsed laser can generate smoothing effects and improve the surface finish [18]. They did not provide any information about the effect of the pulsed regime of the laser on the microstructure, and segregation as well as mechanical properties. Xiao et al. 2017 studied the effect of the laser modes (continuous and pulsed waves) on Nb segregation and Laves formation during laser deposition of Inconel 718. They claimed that the pulsed regime promoted the formation of fine equiaxed dendrites, reduced Nb segregation, and fine discrete Laves phase due to the high cooling rate [19]. Further studies of Xiao et al. 2017 of the continuous and pulsed regime of the laser during metal deposition, highlighted that the samples produced via QCW responded better to the heat treatment and, therefore, higher hardness values were achieved [20]. Recently, Xiao et al. 2020 investigated the effects of two different frequencies when the pulsed laser was used to deposit the Inconel 718. They noticed finer microstructure and more randomly distributed segregated regions when low frequencies were used. In particular, two values of frequencies were investigated but no comparison was carried out with the continuous wave laser mode [21]. Janaki Ram et al. 2013 showed that the current pulsing during the Inconel 718 Gas Tungsten Arc Weld can control the Laves phases, and in particular its morphology (long chains of interconnected Laves phase versus smaller and well separated

interdendritic region) [22]. Wang et al. 2017 observed a higher ultimate tensile strength of the samples produced by pulsed regime laser metal deposition, than the ones produced by the continuous wave laser mode. They also tested different values of duty cycle (interval of time in which the pulse is on or off), however, the results are related to stainless steel (AISI 316L) [23]. Finally, an interesting study has been carried out by Li et al. 2017 that describe, through numerical simulation, how the pulsed or continuous laser affects the thermal field, as well as the melt pool, its shape, and the microstructure [24]. Although the study showed interesting results in terms of microstructure changes and hardness due to the different laser regime, no results depending on the different frequency of pulsed laser were reported. In the previously mentioned works, the authors used a pulsed regime, but the process parameters were different and although they observed similar phenomena, the results were slightly different from each other suggesting that the pulsing parameters affect the process. Therefore, this work aims to assess the effect of different pulse frequencies of the laser on the microstructure, as well as on the segregation distribution of the Inconel 718 thin walls produced by DLD. A comprehensive analysis of the morphology and texture of the grains carried out by electron microscopy is reported and discussed. The results obtained by the thermal analysis are used to discuss the surface roughness, and the melt pool changes due to the process parameter modification (pulsed laser frequency). Moreover, the mechanical properties in terms of microhardness analysis are shown and correlated with the microstructure and the pulse frequency.

2. Material and Methods

The gas-atomised IN718 powder supplied by LPW (Carpenter Technology Corporation) was employed in this experimental work, and the certified chemical composition is reported in Table 1. The average particle size of the powder is 85µm, with 90% of the particles falling within the size range of 43–106µm. As showed in Fig. 1a, the powder particles are mostly spherical, showing some fine satellite particles. Analysing the cross-section (Fig. 1b), some internal porosities were also observed, and this is typically due to the production process (gas atomisation). The analysis of the cross-section is shown in Fig. 1b and the microstructure was revealed and characterized by dendritic morphology. The powder was characterized by fine dendritic networks, which was caused by the rapid solidification experienced by the material during the gas atomisation process. Moreover, through the Energy Dispersive X-ray (EDX) analysis, the white regions were mainly formed by Nb and Mo, suggesting that the segregated regions already existed in the powder (Fig. 1c). The DLD process has been performed to produce single thin-walled samples of dimensions 20mm×25mm along z and x directions respectively and 1.4mm thickness (y direction) on an Inconel 718 substrate (Fig. 2a). The choice of the material substrate was related to the possibility to test the process parameters for repairing actions usually performed on aerospace components.

Table 1. IN718 powder chemical element (w%).

Ni	Cr	Fe	Nb	Mo	Ti	Al	Si	Ta
54.45	18.18	18.19	4.88	2.9	0.91	0.42	0.03	0.02

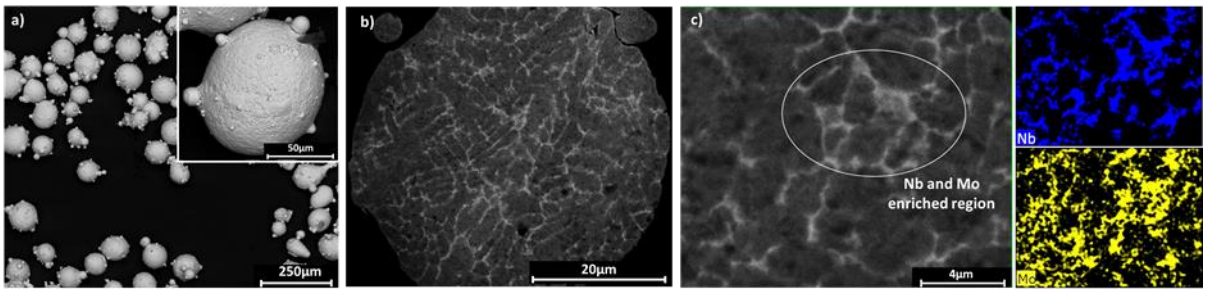

Fig. 1. SEM of the IN718 powder (a); SEM of the cross-section of the powder(b); EDX of the cross-section of the powder (c).

The Trumpf TLC 1005, equipped with an Nd: YAG laser and 1064nm wavelength (maximum power of 4kW) was used to deposit the thin walls in an argon atmosphere within a plastic customized box. During the deposition, the O_2 level was monitored, and a constant flow of argon was used inside the deposition area to keep the O_2 level under 50 ppm value. The layer thickness was kept equal to 0.5mm throughout the build. The argon was also delivered as a carrier gas with a flow rate of 10L/min, and a nozzle gas protected the lens from the rebounding particles from the build. The laser beam was focused to have a spot size of 0.9mm, with a focal length of 127 mm and the power set was equal to 300W. A three-beam nozzle assembly was used for powder feeding, where the distance of the powder focus was set at 2mm under the surface of the substrate, while the laser beam focus was set 2mm above from the substrate. This configuration of the laser and powder focus achieved an auto-compensation of the deposited material, therefore possible irregular deposited layers were avoided [25].

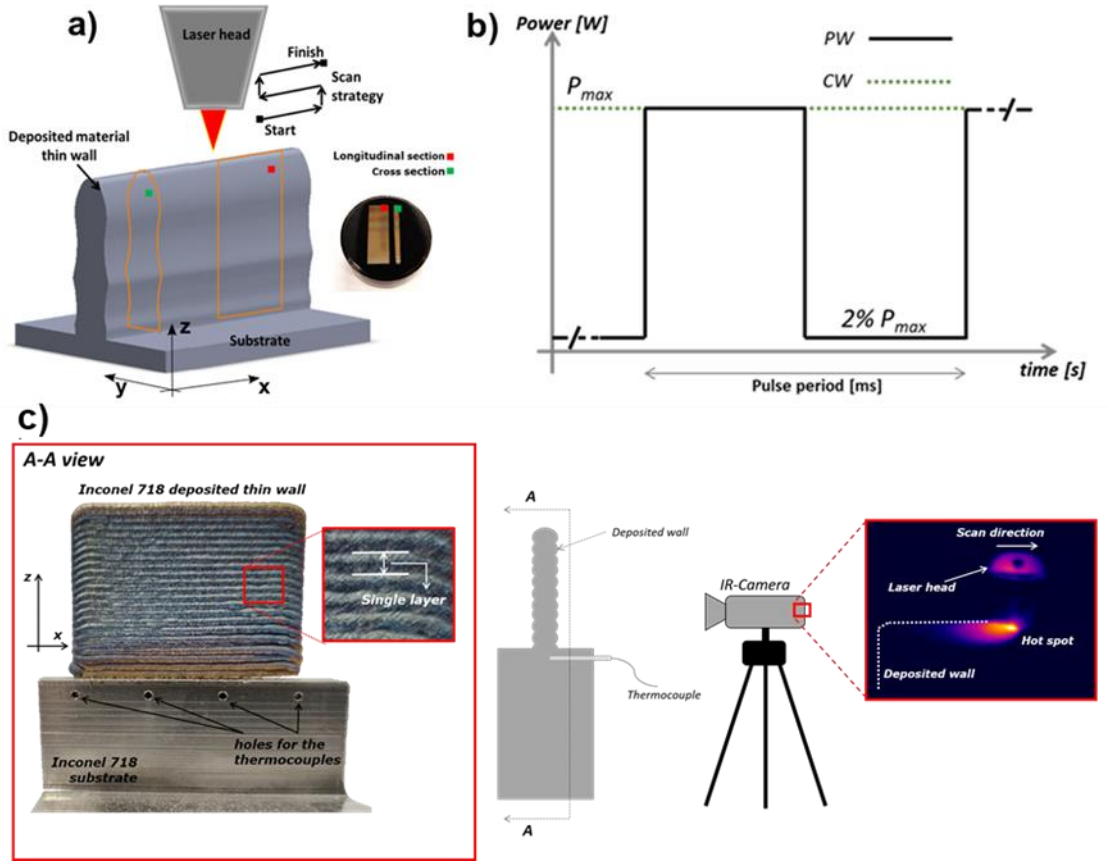

Fig. 2. a) Schematic representation of the thin wall, the deposition strategy and the samples collected; b) pulsed wave and continuous wave graph; a schematic representation of the experimental set-up (c).

The strategy of the deposition was defined as continuous deposition (Fig. 2a), and the scan speed of the laser head at 275mm\min was kept constant for all the tests. As previously mentioned, the laser device was able to work in a pulsed wave regime (PW) (Fig. 2b), therefore, three frequencies of pulsed regime were defined and set equal to 10Hz, 100Hz and 1000Hz and a further deposition with a continuous wave regime (CW) was performed for comparison. Moreover, the thermal field was also investigated by an infra-red camera, positioned in front of the substrate during the deposition, and three thermocouples (K-type) were located 1mm beneath the surface substrate (Fig. 2c). The temperature of the first deposited layers acquired by the thermocouples was compared with the thermal profile

obtained by the infra-red camera. The obtained thin walls were collected and sectioned as showed in Fig. 2a for metallographic and hardness analyses. The surface quality in terms of surface roughness S_a of the side face of each thin wall, was evaluated by the Alicona Infinite Focus G5 plus. The cross and longitudinal section samples (cross and longitudinal section) were embedded in a phenolic resin, subsequently ground and polished, and electro-etched (8V for 10s) using H_3PO_4 electrolytic solution to reveal the microstructure a well as the segregations. Back Scattered Electron Microscopy (BSEM) and Energy Dispersive X-ray diffraction (EDX) analyses were both carried out to characterize the microstructure and the segregation. Furthermore, to evaluate the melt pool boundary, an Optical Microscope (OM) was also used to analyse the samples. The latter analysis was performed after the samples were chemically etched by the Kalling's n.2. The microhardness was measured using a micro indenter (Buehler Wilson VH1202), using a load of 500g with a dwell time of 10s and ten indentations were carried out in each region of the sample analysed, with a total of 30 indentations per sample. Finally, the average value for each region analysed was considered.

3. Results

3.1. Thermal Analysis of the Deposited Thin Walls

The thermal analysis aimed to evaluate the thermal profile during the deposition, and the temperature distribution on the entire deposited parts depending on the process parameters set, for example laser mode and frequencies. The thermal analysis results were reported in Fig. 3. This demonstrates in detail the temperature cycle on a single point positioned in the middle region of the wall, and the comparisons among the CW and the different frequencies of the pulsed laser are also shown. Fig. 3b represents the portion of the graph where the heat

source hits the node considered in the grid and defined on the software used to analyse the file acquired by the infrared camera.

It is possible to note that the fluctuation of the thermal field signals, due to the nature of the heat input, showed the same frequency (10Hz) of the heat source (laser) as also highlighted by Fig. 4. The temperature fluctuations at higher frequencies of the pulsed laser were difficult to capture by the camera due to the low frame per second acquisition rate of the camera. Fig. 3c shows the average temperature measured within the thermal peak. The higher fluctuation, due to the lower frequencies of the pulsed laser, is also highlighted by the standard deviation. The standard deviation becomes smaller when the frequency of the pulsed laser increases due to the higher heat input, and less heat dissipation. Moreover, increasing the frequency of the pulsed laser till the CW laser mode the temperatures increased from 1435°C (10Hz) to 1898°C (CW).

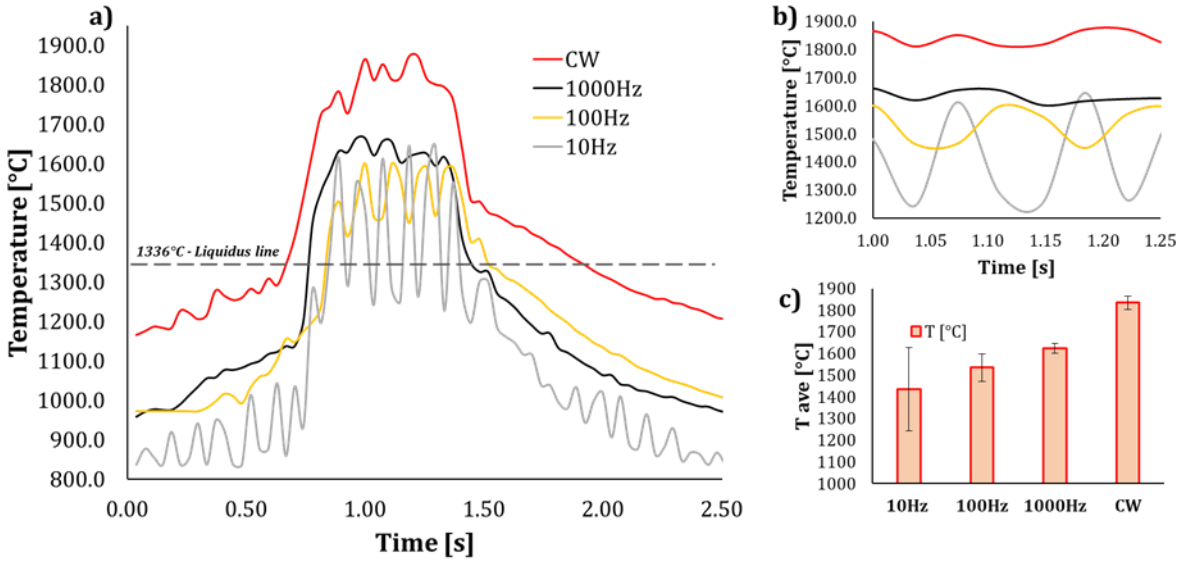

Fig. 3. a) single-point temperature profile within the middle region of the wall; b) temperature profile within the thermal peak zone; c) average temperature evaluated within each thermal peak region.

Fig. 4 shows the comparison between the temperature registered on the melt pool when CW and 10Hz PW laser are used. The temperature measured when the CW laser was used is almost constant and the average value was approximately equal to 1900°C. The slight oscillations were due to the random sparks caused by the partially melted powders expulsed by the melt pool because of the turbulence that developed. The black curve represents the pulsed laser (10Hz) and the dark orange curve represents the temperature profile measured considering the maximum thermal signal within the melt pool. The melt pool was subjected to a continuous heating, and cooling cycle due to the pulsed laser. When the laser went from ON to OFF, the temperature within the melt pool decreased from almost 1700°C to values lower than 1300°C. This result highlights that lower temperatures were achieved with the use of pulsed laser, and thus local thermal cycles within each layer happened during the deposition process. On the contrary, the CW laser mode induced the thermal cycles layer by layer as showed in Fig. 3a.

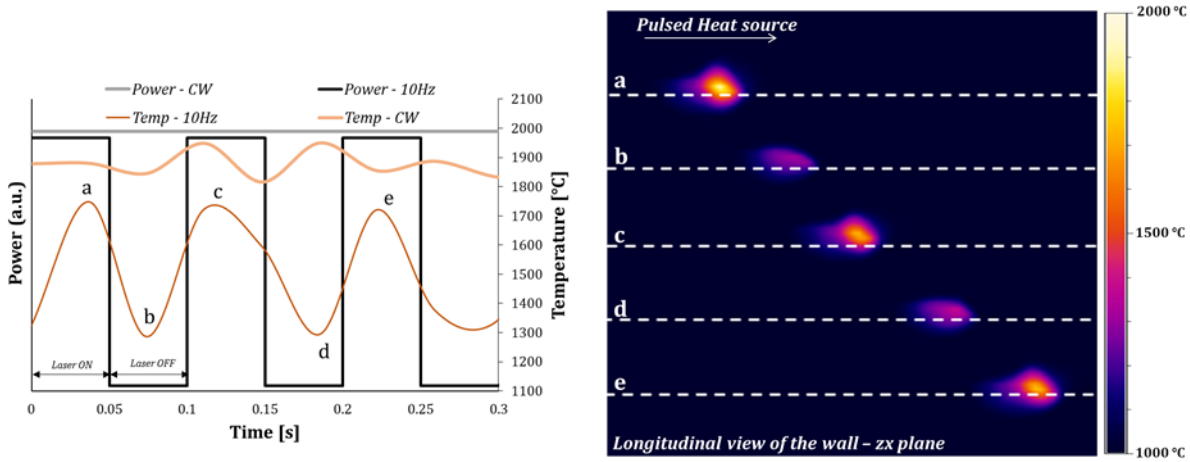

Fig. 4. Temperature profile related to the laser power mode and “heartbeat” effect evaluated by the infrared camera.

In Fig. 5 illustrates the temperatures acquired by the thermocouple during the entire deposition process. The CW allowed higher temperatures to be reached compared with the pulsed laser, and a decreasing of the temperature was observed while the frequency decreased from 1000Hz to 10Hz due to the higher cooling rate was observed. A detailed analysis of the temperature profiles had been carried out (A box) to better evaluate the maximum peak temperatures measured during the deposition. Increasing the frequency of the PW laser until the CW laser regime led to an increase of the accumulated temperature, indeed the evaluated values are 232°C, 241°C, 258°C and 342°C for the 10Hz, 100Hz, 1000Hz and CW respectively.

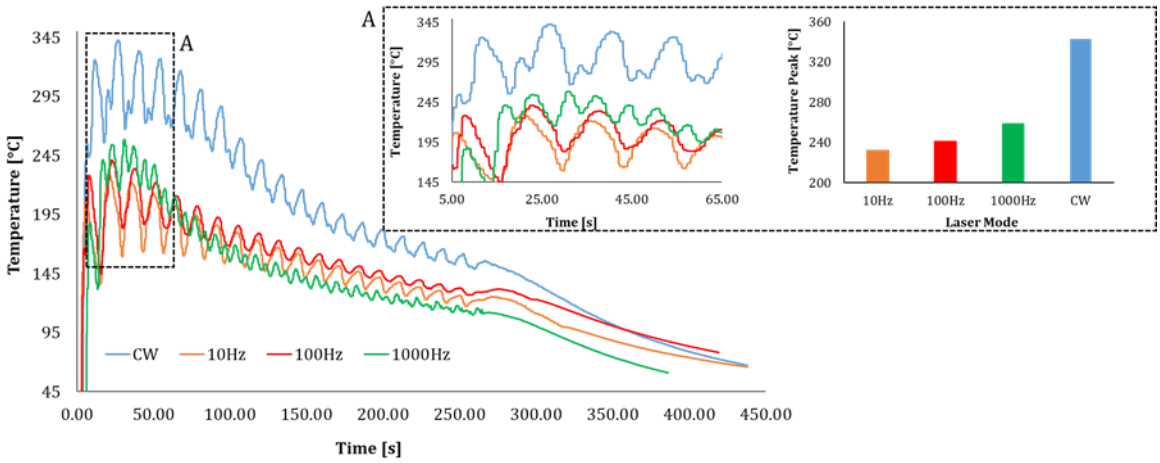

Fig. 5. Temperature profiles acquired by thermocouple during the entire DLD process depending on the laser mode used (CW or pulsed).

3.2. Surface Quality and Microstructure Analysis

The side surface of each wall has been analysed by the SEM and the results are shown in Fig. 6. Each picture refers to the z-x plane and two main features are distinguished: the appearance of the different layers that characterize the walls, and the amount of the

unmelted particles. In general, the number of unmelted particles was lower when the PW laser (Fig. 6a, 6b and 6c) was used instead of the CW (Fig. 6c).

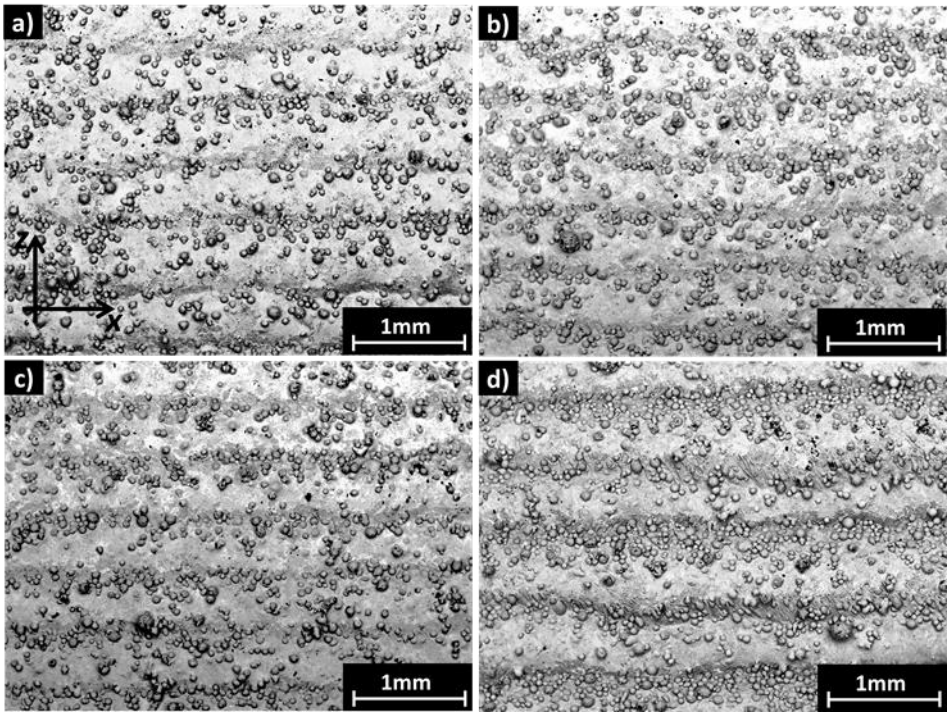

Fig. 6. SEM of the z-x plane of the thin walls; a) 10Hz, b) 100Hz, c) 1000Hz and d) continuous wave.

The surface roughness (S_a) of the side surface of the produced samples has also been measured and the results are reported in Fig. 7.

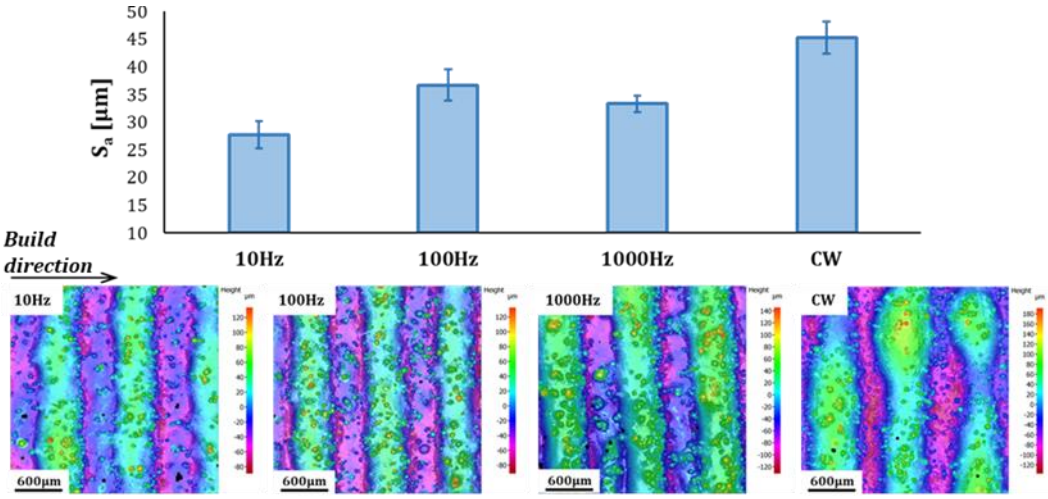

Fig. 7. Surface roughness analysis carried out on the walls produced by PW and CW laser mode.

The surface conditions were affected by the frequency set during the deposition, indeed the pulsing laser perturbs the melt pool, as well as the powder flow that crosses the laser beam. The lower frequency (10Hz) led to better surface roughness of 27µm, while increasing the frequency to 1000Hz and the CW regime, the surface roughness increased up to 46µm.

Fig. 8 shows the microstructure observed by optical microscope on the cross and longitudinal section of the thin walls produced by PW and CW laser mode. In Fig. 8a, 8c, 8e and 8g the melt pool on the cross-section is highlighted by the dashed white lines, to highlight the changes at the various value of frequency. On the longitudinal sections (Fig. 8b, 8d, 8f and 8h) the deposited layer, the growth direction of the grains and the discrete melt pool bands are visible. It is possible to notice that the layer bands depicted by the horizontal dashed lines are approximately 0.5mm thick, especially when the PW laser is used, while the samples produced by CW laser mode showed thicker layer bands of approximately 0.57mm. The discrete melt pool bands are clearly evident when the 10Hz frequency was used, while higher frequencies involved more laser on-laser off cycles per unit time making difficult the

formation of the bands. On the contrary, when the CW laser is adopted, the discrete band is not expected due to the constant presence of the heat source, and indeed it was not visible in the longitudinal section (Fig. 8b). Moreover, from Fig. 8 it is also possible to notice that few pores are randomly distributed as see along the cross-sectional and the longitudinal sections of the thin walls. The porosity analyses carried out by imaging analysis did not show any significant variation between the walls produced with different pulsed laser frequency and also between the continuous and the pulsed laser mode. Therefore, the frequency of the laser did not affect significantly the porosity, keeping the porosity fraction at < 0.95%.

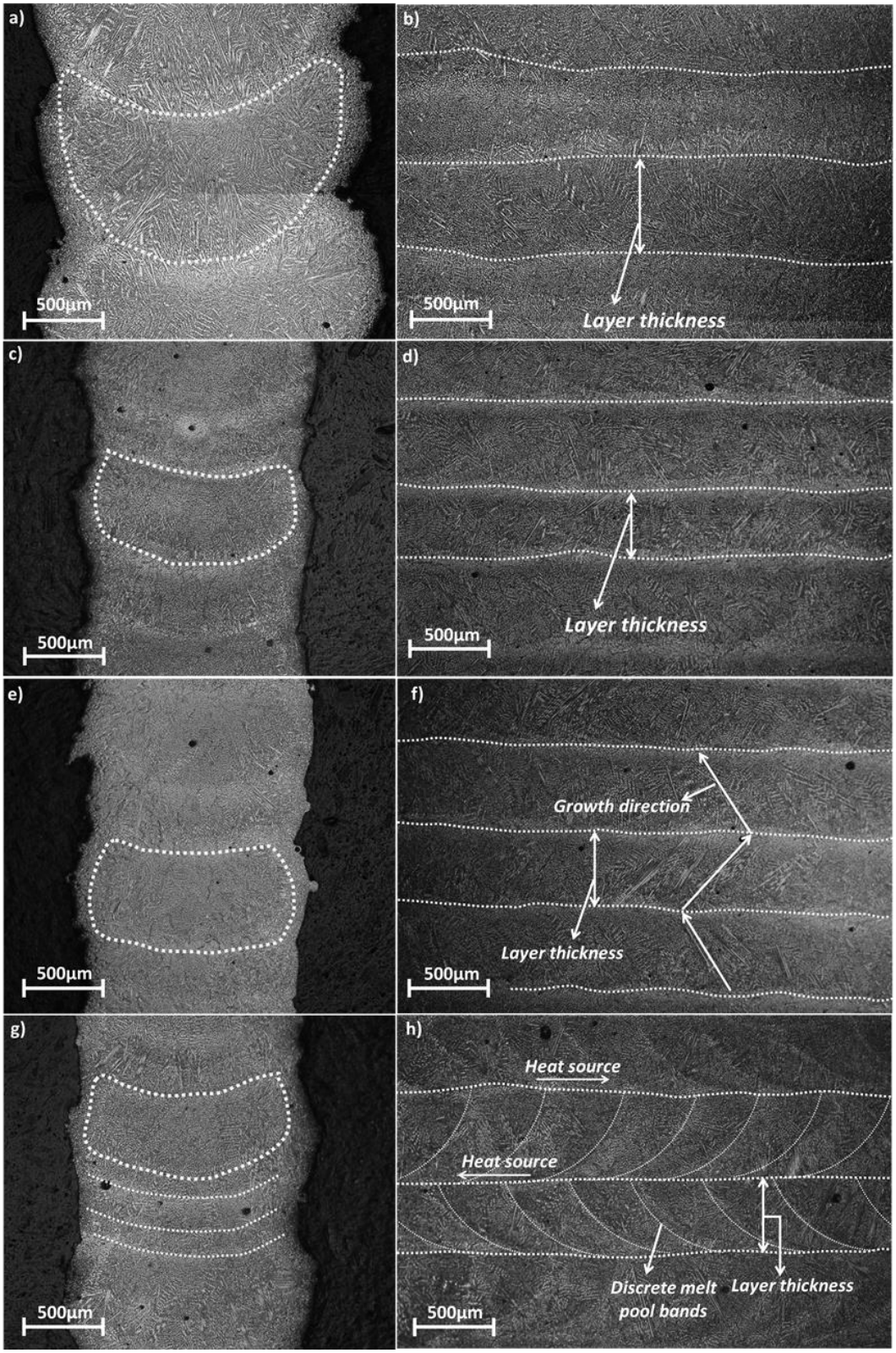

Fig. 8. Cross-section of the thin walls a) CW, c) 1000Hz, e) 100Hz, g) 10Hz; longitudinal section of the thin walls b) CW, d) 1000Hz, f)100Hz and h) 10Hz.

The EBSD maps are reported in Fig. 9 and show the orientation of the crystals, as well as the shape of the grains on the cross and longitudinal section. The orientation of the grains suggests the deposition strategy adopted, continuous from left to right and vice versa since they grew following the heat source. Although this effect is mainly evident when the PW laser is at a high frequency (1000Hz) and CW laser are employed (Fig. 9a and 9b). The use of 100Hz showed a transition from random to zig-zag distribution, whereas the lowest frequency (10Hz) allowed a random distribution of the grains. Indeed, no preferential growth orientation was highlighted by the EBSD map (Fig. 9c).

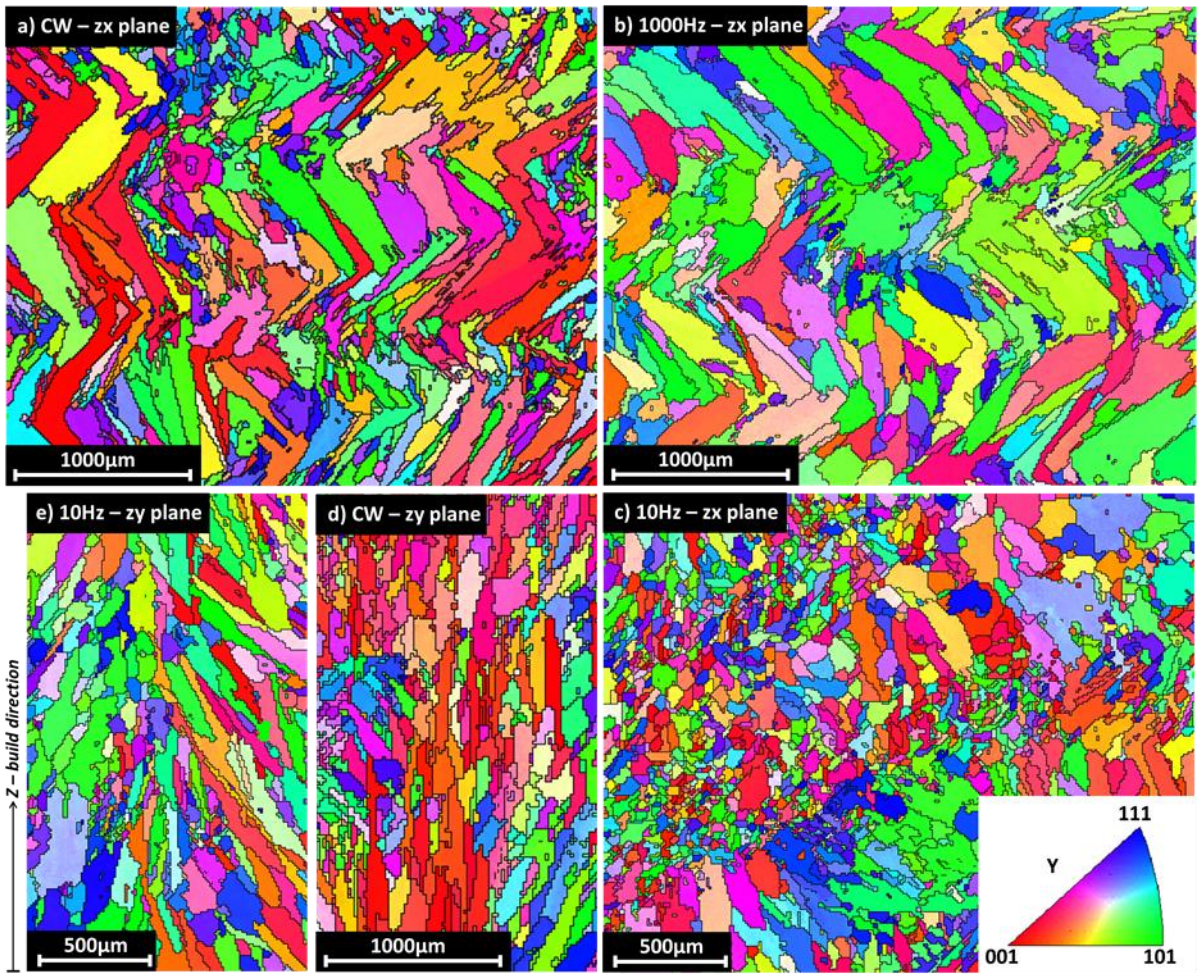

Fig. 9. EBSD map of the longitudinal section zx plane ((a), (b) and (c)), cross section of the thin walls ((d) and (e)).

Moreover, the cross-section of the samples produced by CW laser showed grains mainly oriented to the <001> direction, while although more random distribution was obtained when the PW laser was used at 10Hz frequency (Fig. 9e and 9d).

The primary dendrite arm spacings (PDAS) have been measured on the cross-section of each sample produced, depending on the frequency of the PW laser, and compared with the one related to the sample produced by CW laser (Fig. 10). The 10 measurements per area were taken within three regions; top, middle, and bottom of each wall and for each region the average value was considered. Fig. 10 shows the variation of the microstructure among the "bottom", "middle" and "top" regions of the thin walls cross-region (z-x section). The example of how the PDAS measurement was performed is also shown and the results of the average measurements collected within the three regions mentioned are also reported in the graph (Fig. 10). Although the results show similar trends, the most significant difference is in the middle of the wall, indeed the PDAS measurements are quite different depending on the laser mode used, and the frequency applied. Moreover, the 10Hz frequency produced walls where the PDAS showed a trend from the bottom till the top of the wall that was quite different from the other trends registered. It is important to highlight that there is a difference of approximately 1µm considering the PDAS between the middle region and the top/bottom, when CW laser and the PW (1000Hz, 100Hz) are used. On the contrary, the use of PW laser with a frequency of 10Hz did not significantly affect the microstructure size. (Fig. 10).

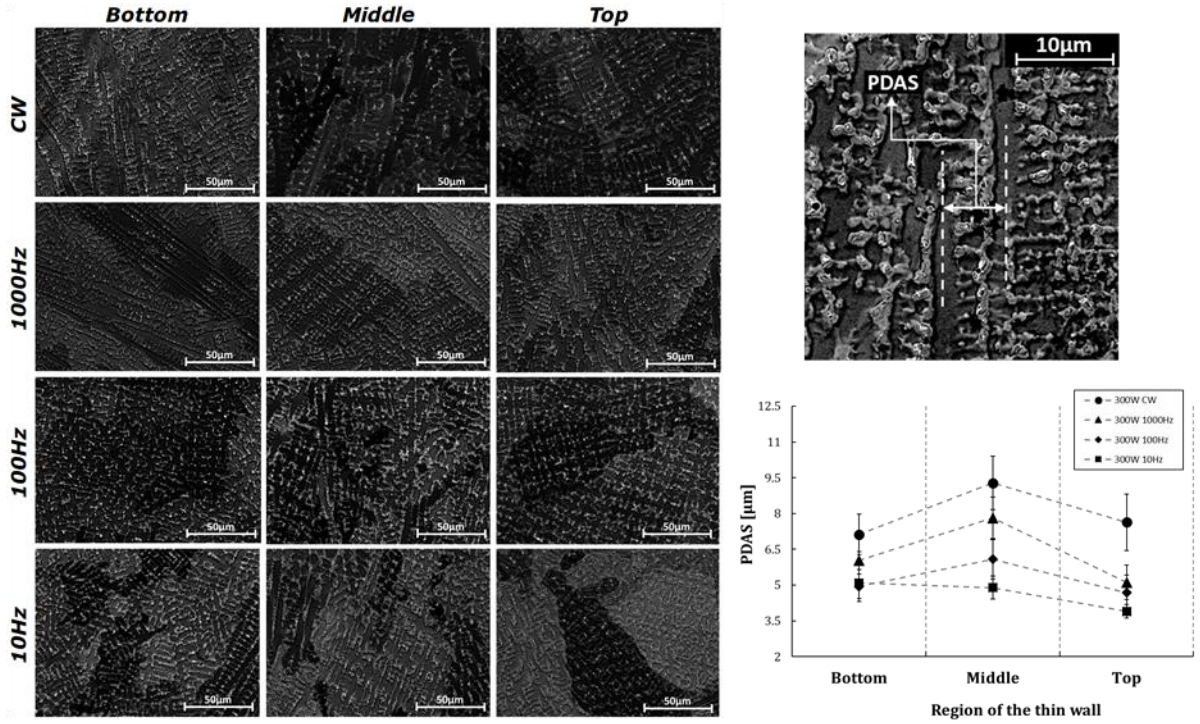

Fig. 10. SEM of the cross-section of the thin walls depending on the frequencies and PDAS measurement.

3.3. Segregation Analysis

The EDS analysis was performed on the cross and longitudinal section of each wall to characterize the segregation regions highlighted by the BSEM analysis (Fig. 11). As expected, the white spots; material with higher atomic density, are mainly composed by Mo and Nb, chemical elements that mainly characterize the Laves phase in the Inconel 718 [8]. Indeed, the redistribution coefficient of the Nb and the Mo is lower than 1, and suggests that they easily segregate in the liquid region and remaining there during the solidification.

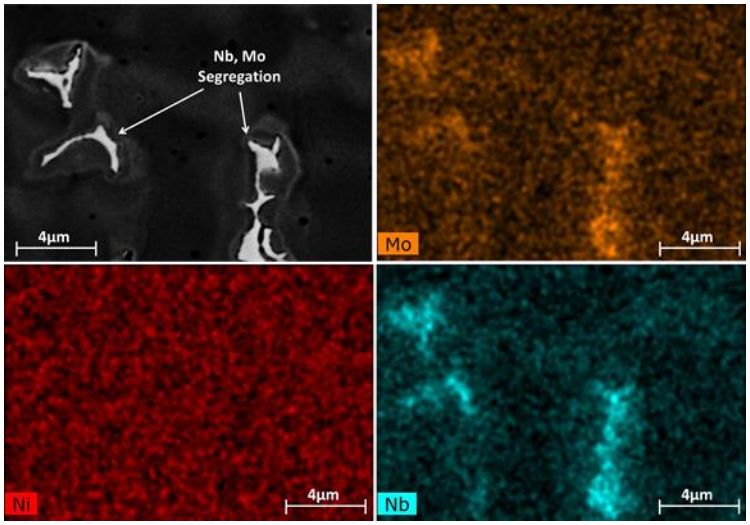

Fig. 11. BSEM of the segregated region and the EDS analysis of the white spots.

To calculate the area of the segregated regions within the cross-section of each sample, several greyscale micrographs were converted in black and white two channels through the threshold level regulation (Fig. 12). In these new pictures (Fig. 12b) the segregated regions were in black, while the γ matrix was white, therefore, the percentage area could be easily calculated. An example of the adopted technique is reported in Fig. 12b, and the collected results were reported in a graph showed in Fig. 13.

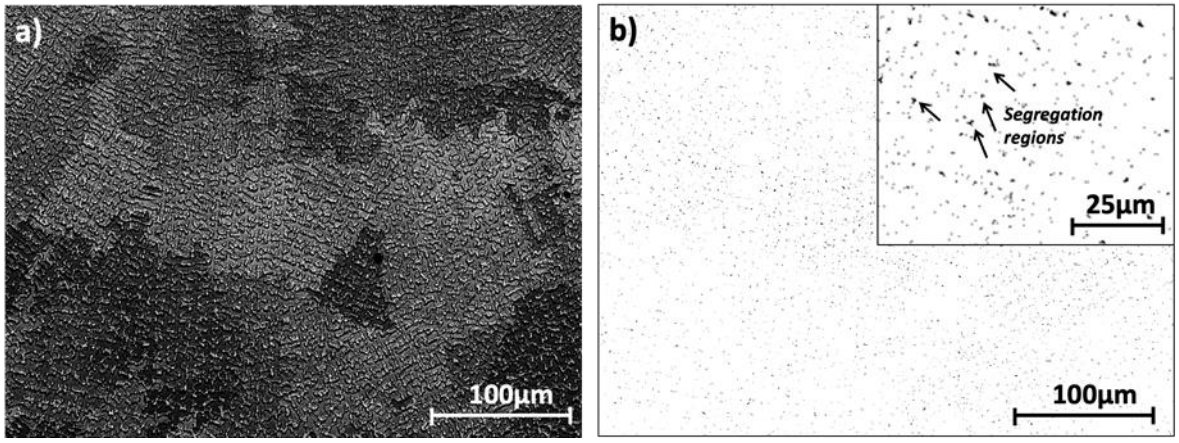

Fig. 12. a) BSEM micrograph of the thin wall cross-section; b) threshold set on picture (a) to balance the black-white level and measure the %area of the segregated regions.

The %area of segregation did not show a significant difference between the bottom and the top of the thin walls when the PW laser with the frequency of 100Hz, 1000Hz or CW laser mode was used. Indeed, the trends were quite similar if compared each other. On the other hand, decreasing the frequency to 10Hz permitted a reduction in the area of the segregation, and keep the distribution almost similar from the bottom till the top of the thin walls (Fig. 13).

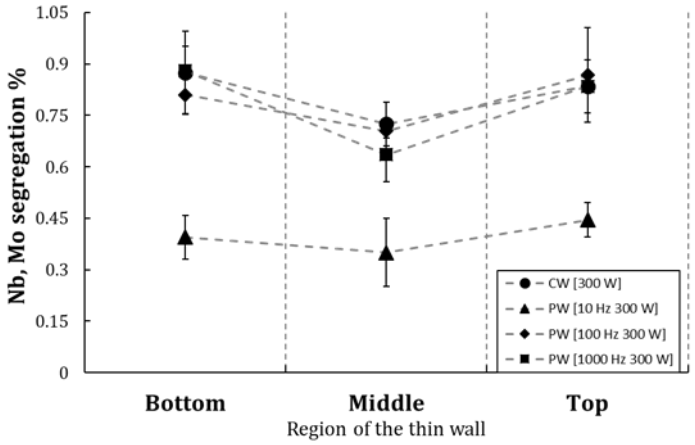

Fig. 13. %Area of the segregated region measured in the bottom, middle and top region of the thin walls cross-sections.

3.4. Hardness Analysis

The microhardness on the cross-section of each wall was measured and the results reported in Fig. 14 and Fig. 15. The gradient map showed that the hardness values were different depending on the height of the deposited walls, and that frequency also played an important role. To quantify the average value of hardness for each wall, the region of interest considered has been divided into three parts starting from the bottom of 0mm to 6mm, and then from

6mm to 14mm and the last part from 14mm to 19mm of the height. The results are shown in Fig. 15.

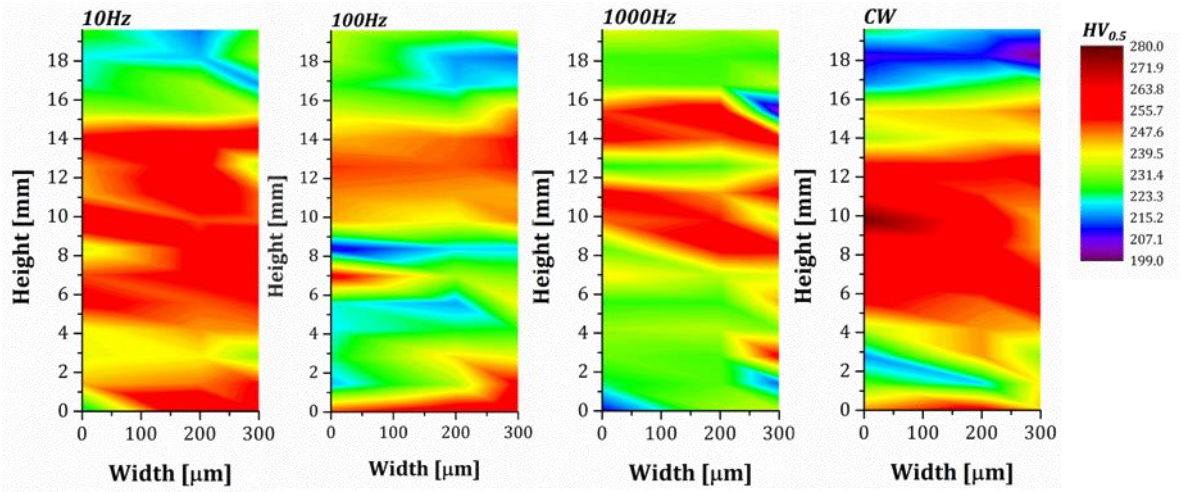

Fig. 14. Hardness measurements of the cross-section of the thin walls (gradient map).

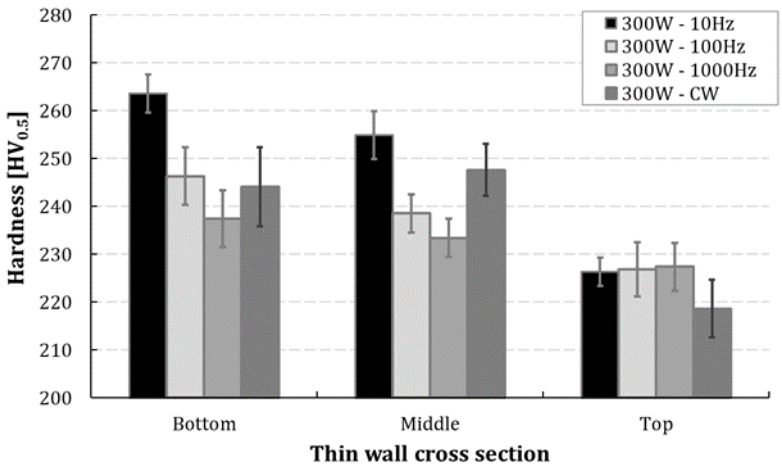

Fig. 15. Hardness average values measured within the cross-section.

Regardless of the PW or CW laser mode used, the hardness trend among the samples analysed did not show any significant changes. In general, the hardness was higher on the bottom and the middle part of the deposited wall and continued to decrease in the top part.

4. Discussion

4.1. Effect of Pulsing Frequency on the Thermal Gradient

The laser mode used during the DLD showed a significant effect on the thermal field. This developed due to the interaction among the powder, heat source and substrate seen in the initial steps of the deposition. The transition of the frequency from 10Hz to 1000Hz of pulsed laser was used until the CW showed an increment of heat within the melt pool, and in general in the overall deposition process. The use of the pulsed laser showed a melt pool characterized by a "heart-beat" behaviour, and, therefore, the development of local thermal cycles (Fig. 3a, Fig. 4 and Fig. 16. A higher frequency (e.g. 1000Hz) led to a thermal field comparable with the CW, while the transition frequency was represented by 100Hz. An interesting local thermal cycle was represented by the 10Hz frequency that led to low heat accumulation, a higher cooling rate and, therefore, the melt pool was subjected by local solidification-melting cycles. Fig. 16 shows the comparison between the temperature measured when the CW and the 10Hz pulsed lasers were used during the DLD process. The temperatures are compared with the power signals set on the laser, and the cyclic temperature oscillations are exactly related to the power graph when the pulsed laser (10Hz) was set. Therefore, when a low frequency such as 10Hz is set with 300W of laser power, the material locally undergoes melting and solidification cycles and this effect is subsequently occurs when the next layers are deposited. On the contrary, using higher frequencies such as 1000Hz or CW laser modes results in the local thermal cycles being neglected and underdeveloped. Consequently, the only thermal cycles induced on the material are due to the subsequent deposition of the next layers.

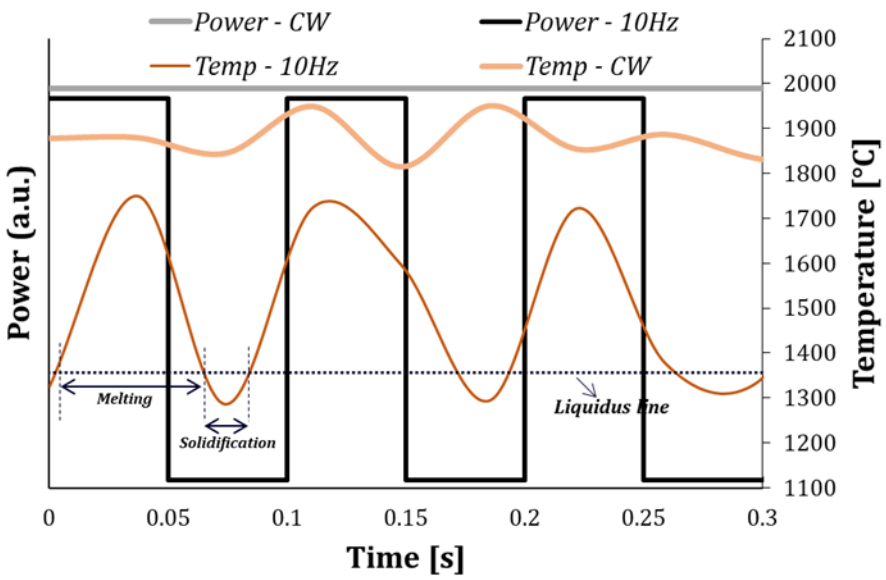

Fig. 16. Comparison of the thermal profiles when pulsed and CW laser modes are used. The use of 10Hz frequency led to local thermal cycles with temperatures between the solidification and the melting region.

Focusing on the pulsed laser, it is possible to summarize that among the three frequencies investigated, the 10Hz reaches an effective cooling rate that leads the temperature to decrease within the solidification region. The cooling rate measured when 100Hz was used, allows the temperature to reach values slightly higher than the melting temperature during cooling when the laser is set on OFF. Therefore, 100Hz represents the transition frequency and a higher value of pulsed frequency which led to thermal field behaviour comparable to the one produced by the CW laser.

Moreover, the thermal field, ten seconds after the deposition process was completed, has also been analysed to qualitatively evaluate the amount of absorbed or dissipated heat. It is possible to claim that the use of a pulsed laser clearly helped reduce the accumulation of the heat in the deposited material, and this result is also evident from the beginning of the manufacturing process as shown by the thermocouples results (Fig. 5). Fig. 17 shows the

distribution of the temperature on the z-x plane of the deposited walls ten seconds after the deposition process was completed. The wall produced by the CW laser showed a higher temperature compared with the ones produced by the pulsed laser. The lower accumulation of heat has been reached by the lower frequency (10Hz) of the pulsed laser (Fig. 17d).

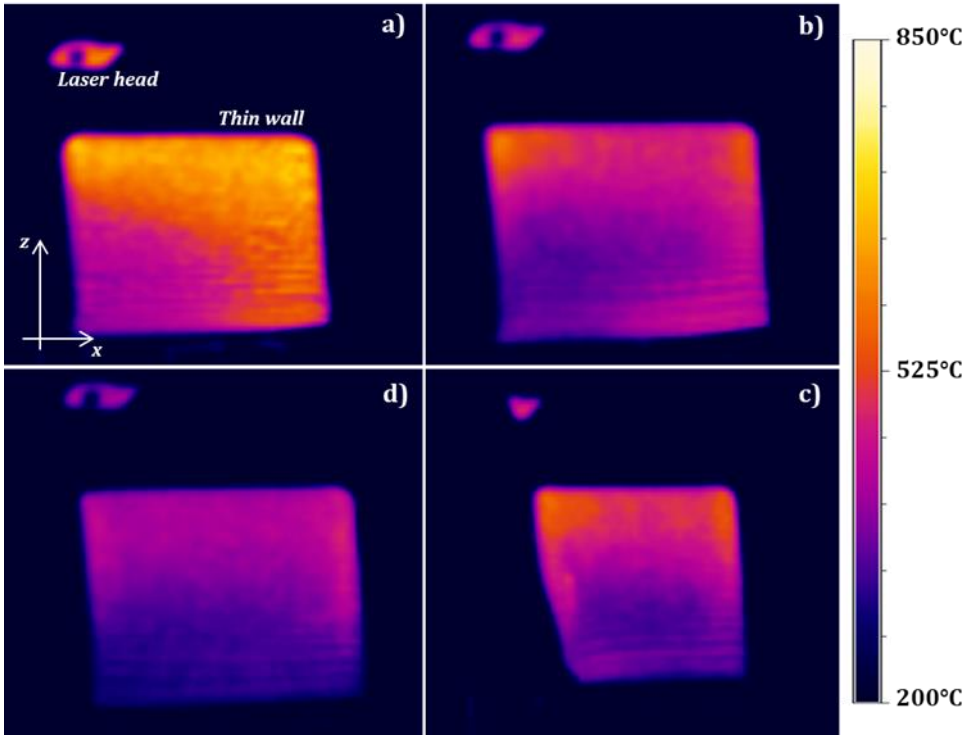

Fig. 17. Temperature distribution on the z-x plane of the thin walls produced by DLD; a) CW laser; b) 1000Hz; c) 100Hz and d) 10Hz pulsed laser.

4.2. Effect of Pulsing Frequency on Surface Quality and Microstructure

Fig. 6 and Fig. 7 show the results of the analyses carried out on the longitudinal surface of the produced walls when different values of the pulsed laser were adopted during the deposition. Focusing on Fig. 6 between each deposited layer there was an accumulation of unmelted powder particles and their accumulation was significant when the frequency was increased

till the CW regime was reached. The surface roughness S_a was also quantified as showed in Fig. 7, and the trend obtained was qualitatively observed also by the SEM analysis. The lowest S_a value measured was 28µm, when the frequency of the pulsed laser was set equal to 10Hz and the S_a increased by 33%, 21% and 63% when the frequency was set equal to 100Hz, 1000Hz and CW respectively.

A similar trend that highlights lower surface roughness when the PW laser is used has been reported by Shah et al. 2010. These quantified results suggest that the increase of the frequency critically increases the surface roughness [26]. The reason for the surface roughness modification was mainly related to the surface disturbance induced by the Marangoni flow, and, therefore, to the mixing and melting of the powder particles within the melt pool. As suggested by Fuhrich et al. 2001, the fluid flow during welding defines the shape of the melt pool. Moreover, the liquid flow pattern is usually produced by the surface tension driven convection known as Marangoni effect [27]. Considering the chemistry of the alloy used in this work, the percentage in weight of S was declared to be equal to 0.015%, which was high enough to lead a positive thermocapillary gradient ($\frac{\partial \gamma}{\partial T}$) [28,29]. A positive thermocapillary gradient provokes a centripetal Marangoni convention, therefore, the positive temperature coefficient of the surface tension led to a significant penetration depth, and a high aspect ratio of the weld pool is usually expected. Fig. 18 schematically reported the cross-section of the walls with the relative melt pool shape when the CW and the 10Hz PW laser were used. In detail, the divergence region of the laser irradiates the melted material, and, therefore, the melt pool, while the powder is blown within this zone. Since the width of the melt pool when using the CW laser was slightly bigger than the laser beam, a cooler region represented by the section ABC was characterized by lower temperature.

Indeed, most of the heat in this region was conducted by the melted material, and not directly by the laser effect. Moreover, due to the positive thermocapillary gradient, a higher surface tension was generated in the region at a higher temperature that corresponded to the centre of the melt pool. Therefore, the combination of the Marangoni flow that pushed part of the peripheral particles. Along with a lower temperature this promoted the accumulation of un-melted particles with consequent formation of a rough surface between the deposited layers as also reported in Fig. 6d.

The use of the pulsed laser during the laser metal deposition resulted in modified melt pool behaviour inducing a high surface disturbance. The high surface disturbance of the melt pool improved the mixing action of the powder within the melt pool, therefore, the powder melted more effectively. Fig. 18 also suggests that the region of the deposited material A'B'C', that was not directly irradiated by the laser beam, and therefore melted, was significantly smaller compared with the one that was formed when the CW laser was used. Consequently, the heat accumulated in this region due to higher conduction, and the particles melted more effectively. Moreover, due to the less energy per time unit generated by the pulsed laser, the temperature peaks were significantly lower, and this reduced the penetration depth leading to a less U shaped melt pool and reduced waviness effect on the external surface (Fig. 6a).

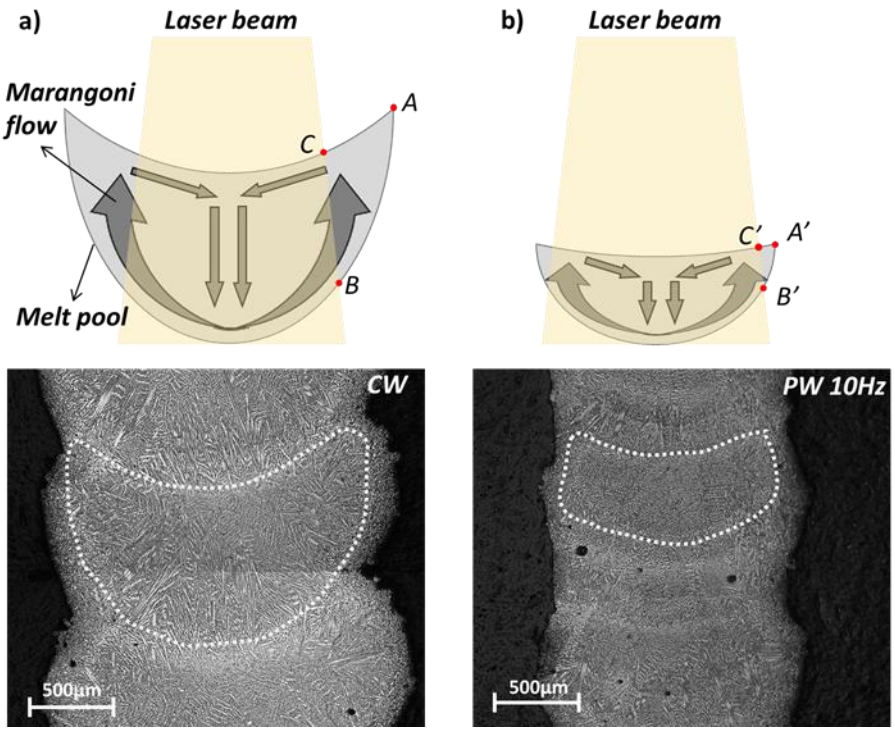

Fig. 18. Marangoni flow within the cross-section of the thin walls when (a) CW and (b) 10Hz PW laser are used.

The different frequencies investigated, and the CW regime of the laser, showed a different effect on the microstructure as reported in Fig. 8, Fig. 9, and Fig. 10. In general, when the laser mode was set as CW, the heat source and the related energy was kept constant during the deposition, therefore, the geometry of the melt pool was not expected to change. Observing the longitudinal section of the thin wall in Fig. 8b, the microstructure grew epitaxially, and the growing direction was dictated by the heat source movement layer by layer. Using the pulsed laser with 1000Hz and 100Hz, a similar development of the columnar dendrites was observed with the CW and is shown in Fig. 8d, Fig. 8f. Moreover, when the frequency was set equal to 100Hz, a slight appearance of the discrete melt pool boundaries was visible, although, they were not clearly distinguishable as showed by Fig. 8h. In detail, since the scan speed was 275mm/min (4.58mm/s), and the pulsing frequency was 10Hz (10 pulse/s) it is possible to

observe that the discrete melt pool band distance, approximately 450µm corresponded to a single laser pulse. Indeed, considering 0.5s, five discrete melt pool bands with a total length of approximately 2.18 mm, should be expected due to the frequency and the scan speed set. In Fig. 8h the five distinguishable discrete melt pool band had a total length of approximately 2.24mm. Considering the orientation of the grains, the dendrites grew differently and were oriented to the centre of each discrete melt pool generated by the pulsed laser. Therefore, it is clear that the pulsed laser, and particularly lower frequency, were able to modify the growing orientation of the dendritic microstructure within the melt pool and layer by layer. The formation of discrete melt pool bands interrupted the formation of long dendrites, since every pulse generated a new melt pool with a new liquid-to-solid, and nucleation of new dendrites from the discrete band (Fig. 8h). The refinement of the microstructure when the pulsed laser was operated, was also clearly confirmed by the EBSD analysis shown in Fig. 9. The use of the CW, and pulsed laser mode (1000Hz) showed similar results in terms of microstructural growth mode and orientation. Indeed Fig. 9a and 9b illustrate a similar zig-zag growing orientation due to the continuous movement of the heat source (laser) from the left to the right and vice-versa. The grains were elongated with a predominant dimension through the build direction (z-direction). Although the predominant size of the grains was comparable with the layer thickness (Fig. 9a) when the laser mode was pulsed, the grains started to show a small refinement (Fig. 9b). This became more significant when the frequency was decreased to 10Hz as showed by Fig. 9c. Therefore, the frequency of the laser played an important role in microstructure refinement. Indeed, the lower frequency, with a more randomly distributed microstructure, with an aspect ratio of the grains very close to 1 enabled a thin part to be manufactured. This latter result was better highlighted by the EBSD carried out on the cross-section of the thin walls (Fig. 9d and Fig. 9e). The grains obtained due

to the 10Hz pulsed laser were more randomly distributed, with no preferential growth direction, indeed in fact the grains were growing among the <001>, <111> and <101> directions. On the contrary, the grains obtained with the CW laser grew more vertically, and showed a preferential growth orientation <001> (crystals in red). The use of low frequency of the pulsed laser completely changed the growth orientation of the grains that are usually driven by the heat source movement. Taking into account the thermal analysis, the higher cooling rate due to the pulsed laser allowed a reduction in heat accumulation, and, therefore, the grains did not have enough time to grow through the preferential orientation driven by the heat source. Indeed, lower frequency means bigger time step during which the laser is off and this corresponds to longer solidification time for the melted material. A significant effect of the solidification time was observed on the sample produced with the lower frequency of the pulsed laser at 10Hz shown in Fig.16. As discussed in paragraph 3.1, higher frequencies than 10Hz showed a thermal field behaviour comparable to the one observed when CW laser was used, and this result explained the slight difference in the microstructure when 100Hz, 1000Hz and CW were used. The microstructural size has been quantified considering the PDAS as showed in Fig. 10. The effects of the heat accumulation and dissipation, and, therefore, the cooling rate, are evident on the size of the primary dendrites. Although the analysis considered the cross-section (z-y plane) of each produced wall, the EBSD analyses highlighted the transition between coarse and fine microstructure on the longitudinal section (z-x plane) when the laser was pulsed with different frequencies. Significant differences in the PDAS started from the middle of the wall till the top, and the different thermal gradient (G) and solidification rate (R) were key factors in this. Chen et al. 2016 [30] investigated the dendritic microstructure behaviour and morphology when DLD was performed with Inconel 718. They used an analytical relation between the PDAS and the cooling rate as showed in Equation 1:

$$\lambda = 80\varepsilon^{-0.33}$$

where λ represents the PDAS and the ε represents the cooling rate ($G \cdot R$) measured in °C/s. Although, the Equation 1 was developed by Katayama and Matsunawa [31] for a laser welded stainless steels, it has been successfully used to estimate the DAS considering different class of materials [30,32]. Manipulating Equation 1 to get the ε value, the cooling rate, depending on the PDAS experimentally measured was reported in Fig. 19. Two different effects, depending on the laser mode used, can be observed by the obtained results. In general, an increase in the cooling rate was due to the decrease of the frequency, and it is also related to the region of the wall considered. The cooling rate obtained with the CW or pulsed laser (100Hz, 1000Hz) showed a similar trend, higher cooling rate in the bottom and top region of the wall. This suggested rapid cooling due to the presence of the substrate, and the air respectively that act as heat sinks. The middle region of the walls showed a lower value due to the accumulation of heat, and this result justify also the coarse microstructure observed within this region. On the contrary, when the 10Hz frequency was used, the cooling rate increased from the boot till the top of the wall suggesting an enhanced dissipation of the heat, and, therefore, finer microstructure as shown by Fig. 10. The cooling rate measured by the thermal field acquired by the infrared camera was compared with the one obtained by the PDAS measurements.

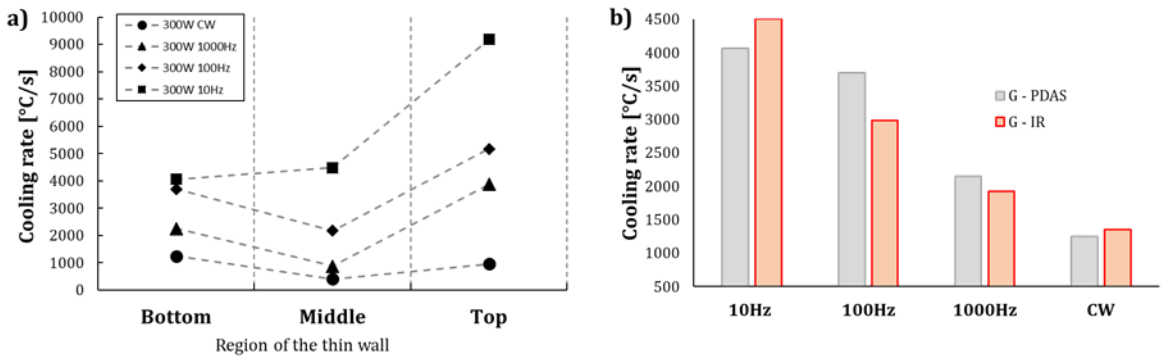

Fig. 19: Cooling rate, a) evaluated by PDAS; b) comparison between the cooling rate evaluated by PDAS and IR camera considering the bottom region of the wall.

4.3. Effect of Pulsing Frequency on Segregation

During the welding procedures or the additive manufacturing process of the Inconel 718 alloy, a particular formation problem of Nb rich phases, known as the Laves phase, is generally experienced. The Laves phase is an intermetallic phase represented by Ni, Cr, Fe_2, Nb, Mo, Ti and its formation is observed within the interdendritic region during the solidification process. This phase is undesirable due to its dual detrimental effects on the mechanical properties. since the Laves phase induces the brittle behaviour and it depletes the γ matrix of useful alloying elements (e.g. Nb and Ti) that forms the strengthening phases (γ' and γ'') after the heat treatments. Moreover, the brittle nature of the Laves phase usually represents a favourable site for cracks formation and propagation [33,34]. In this study, the use of CW and pulsed laser was effective in modifying the segregation morphology in terms of shape and its distribution within the γ matrix. Indeed, the pulsed laser allowed to achieve finer microstructure compared with the CW laser (Fig. 10), therefore, a different distribution of the segregation was also achieved. Moreover, the frequency also played an important role since the PDAS was smaller (10Hz pulsed laser frequency) suggesting finer microstructure. Indeed,

the dendritic grains continuously nucleated and grew, but with limited size due to the fluctuation of the thermal field induced by the pulsed heat source which avoided the development of long columnar grains. The finer microstructure led to the formation of segregation regions more homogenously distributed, while the long inter-connected chains of Laves phase were observed when a higher frequency (1000Hz) and CW laser mode were used. The effectiveness of the heat treatment to drastically reduce or eliminate the segregation regions is usually affected by the morphology of the Laves phase. The exceedingly small Nb-enriched regions with a homogenous distribution showed advantages when the heat treatments (Solution treatment) were performed. This is clearly reported in the literature due to the better diffusion of Nb within the γ matrix to form the strengthening phase γ'' [20]. The morphology changes from inter-connected long Laves phases chains, to very short and isolated segregated regions, was favoured by the pulsed laser due to the combination of cyclic temperatures variations within the melt pool, enhanced cooling rate and fluctuating thermal gradient. Indeed, the interrupted heat source drove the continuous formation of new dendrites nucleation, but with limited size due to the interrupted heat flow. Therefore less Nb was segregated compared to the one observed on the samples produced by a higher frequency or the CW and the segregated regions resulted finer (Fig. 20).

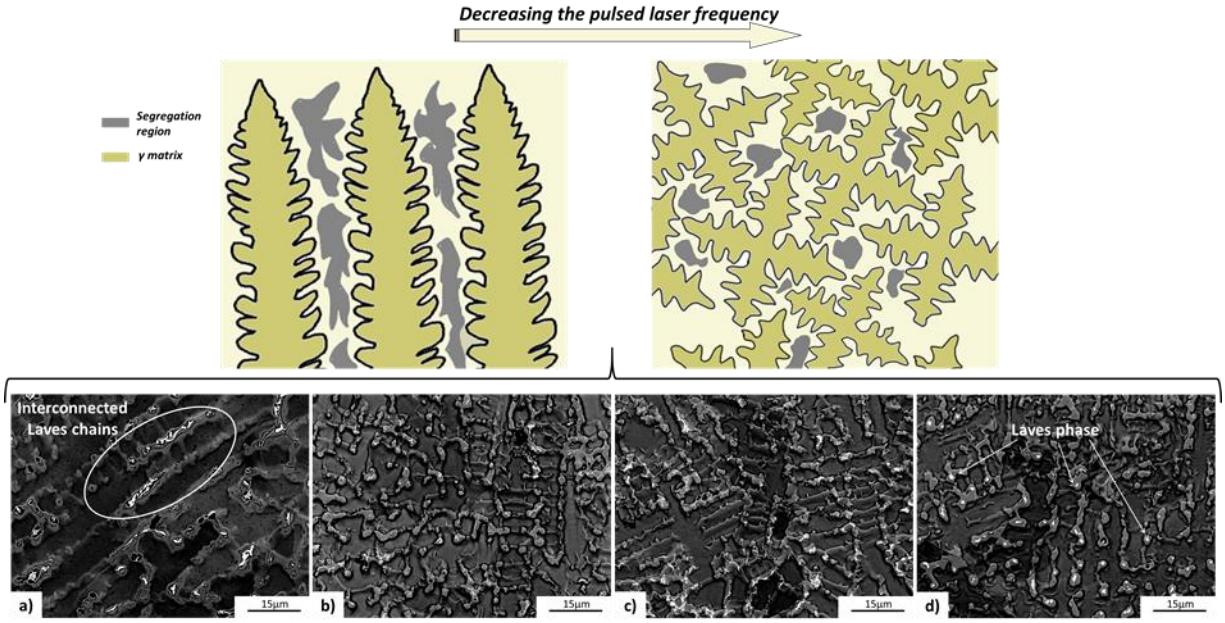

Fig. 20: Variation of the segregation region morphology depending on the pulsed laser frequency; a) CW, b) 1000Hz, c) 100Hz and d) 10Hz.

4.4. Effect of Pulsing Frequency on Mechanical Properties

The micro-hardness analysis carried out on the different samples highlighted some differences as shown in Fig. 14 and Fig. 15. The Inconel 718 is primarily strengthened by the γ'' formation (Ni_3Nb). However, during the DLD process, the rapid solidification does not allow the formation of the γ''-phase resulting in a low strength material. The low hardness values measured shown in Fig. 14 and Fig. 15 demonstrate the strengthening phase γ' was not developed but two main differences can be observed. Firstly, there is a clear difference in terms of hardness distribution when the PW and the CW laser are used to produce the samples. Indeed, as suggested in Fig. 14, the hardness distribution measured on the PW samples were generally high close to the substrate. This decreased gradually reaching the top of the wall, while the one measured on the sample produced by CW, showed a constant hardness distribution and a rapid drop only on the top part. The second difference is evident among the samples produced only by the pulsed laser. As observed, the frequency of the

pulsed laser affected the microstructure, segregation distribution, and, therefore, the hardness. Higher values of hardness were observed in the region of the material where a higher cooling rate, lower heat accumulation, and smaller PDAS were measured (lower frequency of the pulsed laser). Moreover, the sample produced by 10Hz pulsed laser showed almost the same value of hardness within the 14mm of the deposited material. This result highlights that the pulsed laser, and in particular, the 10Hz frequency led to important material enhancements. Indeed the higher and constant cooling rate within the 14mm of the deposited material (Fig. 19a), induced the nucleation and growth of smaller dendrites characterized by similar PDAS values (Fig. 10) and, therefore, higher hardness value. On the contrary, increasing the frequency to 100Hz and 1000Hz, the higher values of PDAS due to the higher heat accumulation and lower cooling rate, unavoidably induced a decrease of the hardness. Moreover, the changing in cooling rate from the bottom to the middle region of the wall, induced a variation in the microstructure size (PDAS), that led to an irregular hardness distribution as highlighted by the coloured map related to the 100Hz and 1000Hz in Fig. 14.

5. Conclusion

In this work, the effect of different pulsed wave laser frequencies, in comparison to continuous wave laser, on the surface roughness, microstructure, segregation and hardness was investigated during DLD. Infrared imaging was used to estimate the cooling rates induced by the laser mode and frequency. The surface quality and the roughness were evaluated by SEM and laser confocal microscopy. Micro-segregation was characterised using SEM and EDX analyses while the microstructure characteristics were analysed using EBSD. The hardness of

the produced parts was assessed by micro-indentation carried out on the longitudinal section of the samples. The main conclusion can be summarised as follows:

1. The thermal field analysis highlights that the use of the pulsed laser allow to reduce the heat accumulated and therefore lower temperature are also involved in the deposition process. Moreover, the use of low frequencies (in particular 10Hz) results in higher cooling rate and localised thermal cycles due to the variable heat source.
2. The surface quality of the produced parts improves when the pulsed laser is used, and better results are achievable with lower frequencies due to the melt pool shape modification. The pulsed laser allows to modify the melt pool shape due to the combination of Marangoni flow, reduce accumulated heat and better mix the particles, resulting in reduced waviness of the external surface (therefore, better surface quality).
3. The PDAS and the grains morphology as well as the orientation growth are affected by different kind of frequencies set when the pulsed laser is used. With the CW and high frequencies (e.g. 1000Hz) the microstructure develops showing a zig-zag growing path drove by the heat source movement. The use of a low frequency (e.g. 10Hz) resulted in a more randomly oriented microstructure. Moreover, the microstructure experienced a transition from finer to coarser with an increase of the frequency to 1000 Hz, as well as through the use of the CW laser mode.
4. The fine microstructure induced by the pulsed wave laser avoids the formation of long interconnected Laves phase chains, resulting in a reduced amount of segregation.
5. The hardness is affected by the use of the different laser modes (i.e. continuous wave or pulsed wave). The use of the pulsed wave enhances the hardness of the deposited material due to the combined effect of the reduced segregated phases and the finer

microstructure. The latter can show a better response to the heat treatment (solution treatment and ageing) as highlighted by the literature.

In future research, the conventional heat treatments such as solution treatment and ageing as well as Hot Isostatic Pressing can be investigated to study their effects on parts produced by pulsed wave laser with different frequencies as well as the continuous wave laser.

Acknowledgments

The authors would like to acknowledge the European research project that founded this research. The project belongs to Horizon 2020 research and innovation programme Novel ALL-IN-ONE machines, robots, and systems for affordable, worldwide and lifetime Distributed 3D hybrid manufacturing and repair operations (Project ID: 723795). AA would like to acknowledge the funding by the Royal Commission of Jubail and Yanbu (Kingdom of Saudi Arabia) for funding his PhD project.

References

[1] C. Chen, H.C. Wu, M.F. Chiang, Laser cladding in repair of IN738 turbine blades, Int. Heat Treat. Surf. Eng. 2 (2008) 140–146. https://doi.org/10.1179/174951508X446484.

[2] A. Weisheit, A. Gasser, G. Backes, T. Jambor, N. Pirch, K. Wissenbach, Direct Laser Cladding , Current Status and Future Scope of Application, in: 2013: pp. 221–240. https://doi.org/10.1007/978-3-642-28359-8_5.

[3] D. Gu, D. Gu, Laser Additive Manufacturing (AM): Classification, Processing Philosophy, and Metallurgical Mechanisms, in: Laser Addit. Manuf. High-Performance Mater.,

Springer Berlin Heidelberg, 2015: pp. 15–71. https://doi.org/10.1007/978-3-662-46089-4_2.

[4] M.J. Donachie, S.J. Donachie, SUPERALLOYS A Technical Guide Second Edition Superalloys: A Technical Guide (#06128G) www.asminternational.org, 2002. www.asminternational.org (accessed June 8, 2020).

[5] F. Campbell, Manufacturing Technology for Aerospace Structural Materials, Elsevier Ltd, 2006. https://doi.org/10.1016/B978-1-85617-495-4.X5000-8.

[6] M. Durand-Charre, The microstructure of superalloys, Gordon and Breach Science Publishers, 1997.

[7] Y. Chen, Y. Guo, M. Xu, C. Ma, Q. Zhang, L. Wang, J. Yao, Z. Li, Study on the element segregation and Laves phase formation in the laser metal deposited IN718 superalloy by flat top laser and gaussian distribution laser, Mater. Sci. Eng. A. 754 (2019) 339–347. https://doi.org/10.1016/j.msea.2019.03.096.

[8] C. Radhakrishna, K. Prasad Rao, The formation and control of Laves phase in superalloy 718 welds, J. Mater. Sci. 32 (1997) 1977–1984. https://doi.org/10.1023/A:1018541915113.

[9] R.C. Reed, The Superalloys fundamentals and applications, Cambridge University Press, 2006. https://doi.org/10.1017/CBO9780511541285.

[10] Z. Li, J. Chen, S. Sui, C. Zhong, X. Lu, X. Lin, The microstructure evolution and tensile properties of Inconel 718 fabricated by high-deposition-rate laser directed energy deposition, Addit. Manuf. (2019) 100941. https://doi.org/10.1016/j.addma.2019.100941.

[11] S. Sui, J. Chen, E. Fan, H. Yang, X. Lin, W. Huang, The influence of Laves phases on the high-cycle fatigue behavior of laser additive manufactured Inconel 718, Mater. Sci. Eng. A. 695 (2017) 6–13. https://doi.org/10.1016/j.msea.2017.03.098.

[12] T. Antonsson, H. Fredriksson, The effect of cooling rate on the solidification of INCONEL 718, Metall. Mater. Trans. B Process Metall. Mater. Process. Sci. 36 (2005) 85–96. https://doi.org/10.1007/s11663-005-0009-0.

[13] Y.C. Zhang, Z.G. Li, P.L. Nie, Y.X. Wu, Effect of ultrarapid cooling on microstructure of laser cladding IN718 coating, Surf. Eng. 29 (2013) 414–418. https://doi.org/10.1179/1743294413Y.0000000142.

[14] H. Qi, M. Azer, A. Ritter, Studies of standard heat treatment effects on microstructure and mechanical properties of laser net shape manufactured INCONEL 718, Metall. Mater. Trans. A Phys. Metall. Mater. Sci. 40 (2009) 2410–2422. https://doi.org/10.1007/s11661-009-9949-3.

[15] M. Ma, Z. Wang, X. Zeng, Effect of energy input on microstructural evolution of direct laser fabricated IN718 alloy, Mater. Charact. 106 (2015) 420–427. https://doi.org/10.1016/j.matchar.2015.06.027.

[16] Y. Zhai, D.A. Lados, E.J. Brown, G.N. Vigilante, Understanding the microstructure and mechanical properties of Ti-6Al-4V and Inconel 718 alloys manufactured by Laser Engineered Net Shaping, Addit. Manuf. 27 (2019) 334–344. https://doi.org/10.1016/j.addma.2019.02.017.

[17] D. Kong, C. Dong, X. Ni, L. Zhang, C. Man, J. Yao, Y. Ji, Y. Ying, K. Xiao, X. Cheng, X. Li, High-throughput fabrication of nickel-based alloys with different Nb contents via a

dual-feed additive manufacturing system: Effect of Nb content on microstructural and mechanical properties, J. Alloys Compd. 785 (2019) 826–837. https://doi.org/10.1016/j.jallcom.2019.01.263.

[18] M. Gharbi, P. Peyre, C. Gorny, M. Carin, S. Morville, P. Le Masson, D. Carron, R. Fabbro, Influence of a pulsed laser regime on surface finish induced by the direct metal deposition process on a Ti64 alloy, J. Mater. Process. Technol. 214 (2014) 485–495. https://doi.org/10.1016/j.jmatprotec.2013.10.004.

[19] H. Xiao, S.M. Li, W.J. Xiao, Y.Q. Li, L.M. Cha, J. Mazumder, L.J. Song, Effects of laser modes on Nb segregation and Laves phase formation during laser additive manufacturing of nickel-based superalloy, Mater. Lett. 188 (2017) 260–262. https://doi.org/10.1016/j.matlet.2016.10.118.

[20] H. Xiao, S. Li, X. Han, J. Mazumder, L. Song, Laves phase control of Inconel 718 alloy using quasi-continuous-wave laser additive manufacturing, Mater. Des. 122 (2017) 330–339. https://doi.org/10.1016/j.matdes.2017.03.004.

[21] H. Xiao, P. Xie, M. Cheng, L. Song, Enhancing mechanical properties of quasi-continuous-wave laser additive manufactured Inconel 718 through controlling the niobium-rich precipitates, Addit. Manuf. 34 (2020) 101278. https://doi.org/10.1016/j.addma.2020.101278.

[22] G.D.J. Ram, A.V. Reddy, K.P. Rao, G.M. Reddy, Control of laves phase in inconel 718 GTA welds with current pulsing, Sci. Technol. Weld. Join. 9 (2004) 390–398. https://doi.org/10.1179/136217104225021788.

[23] X. Wang, D. Deng, H. Yi, H. Xu, S. Yang, H. Zhang, Influences of pulse laser parameters

on properties of AISI316L stainless steel thin-walled part by laser material deposition, Opt. Laser Technol. 92 (2017) 5–14. https://doi.org/10.1016/j.optlastec.2016.12.021.

[24] S. Li, H. Xiao, K. Liu, W. Xiao, Y. Li, X. Han, J. Mazumder, L. Song, Melt-pool motion, temperature variation and dendritic morphology of Inconel 718 during pulsed- and continuous-wave laser additive manufacturing: A comparative study, Mater. Des. 119 (2017) 351–360. https://doi.org/10.1016/j.matdes.2017.01.065.

[25] G. Zhu, D. Li, A. Zhang, G. Pi, Y. Tang, The influence of standoff variations on the forming accuracy in laser direct metal deposition, Rapid Prototyp. J. 17 (2011) 98–106. https://doi.org/10.1108/13552541111113844.

[26] K. Shah, A.J. Pinkerton, A. Salman, L. Li, Effects of melt pool variables and process parameters in laser direct metal deposition of aerospace alloys, Mater. Manuf. Process. 25 (2010) 1372–1380. https://doi.org/10.1080/10426914.2010.480999.

[27] T. Fuhrich, P. Berger, H. Hügel, Marangoni effect in laser deep penetration welding of steel, J. Laser Appl. 13 (2001) 178–186. https://doi.org/10.2351/1.1404412.

[28] P.D. Lee, P.N. Quested, M. McLean, Modelling of Marangoni effects in electron beam melting, Philos. Trans. R. Soc. London. Ser. A Math. Phys. Eng. Sci. 356 (1998) 1027–1043. https://doi.org/10.1098/rsta.1998.0207.

[29] Y. Lee, S.S. Babu, D.F. Farson, Influence of Fluid Convection on Weld Pool Formation in Laser Cladding Solidification Microstructure Control in Electron Beam Additive Manufacturing View project, n.d. https://www.researchgate.net/publication/268278864 (accessed June 8, 2020).

[30] Y. Chen, F. Lu, K. Zhang, P. Nie, S.R. Elmi Hosseini, K. Feng, Z. Li, Dendritic microstructure

and hot cracking of laser additive manufactured Inconel 718 under improved base cooling, J. Alloys Compd. 670 (2016) 312–321. https://doi.org/10.1016/j.jallcom.2016.01.250.

[31] S. Katayama, A. Matsunawa, Solidification microstructure of laser welded stainless steels, (1984) 60. https://doi.org/10.2351/1.5057623.

[32] J.N. Dupont, C. V. Robino, A.R. Marder, M.R. Notis, Solidification of Nb-bearing superalloys: Part II. Pseudoternary solidification surfaces, Metall. Mater. Trans. A Phys. Metall. Mater. Sci. 29 (1998) 2797–2806. https://doi.org/10.1007/s11661-998-0320-x.

[33] S.G.K. Manikandan, D. Sivakumar, M. Kamaraj, Welding the inconel 718 superalloy: Reduction of micro-segregation and laves phases, Elsevier, 2019. https://doi.org/10.1016/C2018-0-01653-9.

[34] J.N. DuPont, J.C. Lippold, S.D. Kiser, Welding Metallurgy and Weldability of Nickel-Base Alloys, John Wiley & Sons, Inc., Hoboken, NJ, USA, 2009. https://doi.org/10.1002/9780470500262.